

Anti-diffusive, Non-oscillatory Central (*adNOC*) scheme to solve the shallow water equations over an erodible substrate in two dimensions.

Haseeb Zia ^{*†}

Guy Simpson [‡]

November 12, 2019

Abstract

Shallow water surface flows commonly entrain sediments, resulting in scouring and/or deposition of the underlying substrate that may strongly influence the pattern of subsequent flow. These coupled phenomena, which can be investigated mathematically with some extension of the shallow water equations, present numerous challenges for numerical methods. Here, we present a straightforward Riemann-solver free approach to solve these equations based on the explicit non-oscillatory central (NOC) scheme that has already been widely applied to hyperbolic conservation laws in other contexts. Our version of the central scheme is second-order accurate in time and space and is used with an anti-diffusive correction to reduce numerical diffusion usually suffered by central schemes. Numerical experiments show that the scheme is accurate and robust for a range of applications from highly dynamic spontaneous dam break over a mobile bed to slowly evolving morphological bed in an alluvial river.

Key words: Shallow water, Erosion, Deposition, Numerical dissipation, Central schemes, hyperbolic conservation laws.

Introduction

Sediment transport in surface water flows is a subject with considerable importance for environmental and engineering problems and is critical to our understanding and prediction of Earth's surface changes in response to the gradually evolving climate or to catastrophic extreme climatic events. The problem is

^{*}Geo-Energy Lab, Gaznat chair on Geo-Energy, École polytechnique fédérale de Lausanne, EPFL ENAC IIC GEL, GC B1 392 (Bâtiment GC), Station 18, CH-1015 Lausanne, Switzerland. E-mail: haseeb.zia@epfl.ch

[†]Dept. of Earth and Environmental Sciences, Univ. of Geneva, 13 Rue des Maraichers, 1205 Geneva, Switzerland.

[‡]Dept. of Earth and Environmental Sciences, Univ. of Geneva, 13 Rue des Maraichers, 1205 Geneva, Switzerland. E-mail: Guy.Simpson@unige.ch

physically complex since it involves the flow of water that induces erosion or deposition of the underlying substrate, thereby modifying the surface and subsequent flow (Cao and Carling, 2002; Cao et al., 2004; Cao and Carling, 2005; Cao et al., 2011; Hudson and Sweby, 2005; Simpson and Castelltort, 2006; Yue et al., 2008a; Bilanceri et al., 2010; Benkhaldoun et al., 2011; Li and Duffy, 2011; Nicholas, 2013a). From a mathematical point of view, the problem is also challenging for a number of reasons. First, the system of governing equations, usually based on some form of the shallow water equations coupled to sediment transport and bed evolution, is highly non linear and hyperbolic, having solutions exhibiting propagating shocks that can cause numerical instabilities with naive schemes (Toro, 2001; Zoppou and Roberts, 2003). Second, as the water depth approaches zero close to the wet/dry front, it can cause negative water depth due to small numerical oscillations, resulting in break down of calculations (Audusse and Bristeau, 2005; Kurganov et al., 2007; Beljadid et al., 2016). Diminishing water height can also cause the equations to become singular (due to bed friction), which can lead to numerical instabilities (Bradford and Sanders, 2002; Begnudelli and Sanders, 2006; Bollermann et al., 2013a). Third, accurately calculating the seemingly trivial steady state of water body at rest over irregular bottom topography have proved to be challenging. In this case, a delicate balance is required between the flux gradient and the source term in the momentum conservation equation. Even a small imbalance between the two terms results in unphysical spontaneous water movement (the so called numerical storm). Schemes that are able to accurately calculate steady state solution over irregular topography are referred as C-property maintaining or well-balanced schemes (some examples of such schemes are (LeVeque, 1998; Rogers et al., 2003; Castro et al., 2005; Canestrelli et al., 2010; Kesserwani and Liang, 2010; Ricchiuto, 2011; Bollermann et al., 2013a, 2015)). Fourth, if the interaction between the flow of water and evolution of the mobile bed is weak, the characteristic time scales of the flow and of the sediment transport can be very different, causing the equations to become stiff (e.g., see (Bilanceri et al., 2010)), necessitating very small time steps to ensure stability with explicit methods.

In the last few decades, numerous high resolution numerical methods have been developed and applied to solve systems of hyperbolic conservation laws such as the shallow water system (e.g., (Harten, 1983; Sweby, 1984; Toro, 2001; LeVeque, 2002; Jiang and Tadmor, 1998)). Many of these schemes employ the Godunov approach by which the approximate solution is realised by a piecewise polynomial that is reconstructed from the evolving cell-averages. Within the Godunov class of methods, two main approaches can be distinguished: upwind and centered. Many upwind methods evaluate numerical fluxes across cell boundaries using knowledge of the wave structure (given by the eigen values of the Jacobian of the system) in combination with Riemann solvers (e.g., (Cao et al., 2004; Hudson and Sweby, 2005; Simpson and Castelltort, 2006; Yue et al., 2008a; Bilanceri et al., 2010; Benkhaldoun et al., 2011; Li and Duffy, 2011; Nicholas, 2013b; He et al., 2014; Fraccarollo and Capart, 2002; Li and Duffy, 2011)) or ENO or WENO reconstruction (e.g., (Črnjarić Žic

et al., 2004; Castro Díaz et al., 2008)). These methods are often highly accurate, but can suffer from splitting and are less successful in cases where the detailed wave structure of the equations is poorly known (as can be the case for the type of problem investigated here). Centered schemes on the other hand - of which CWENO and NOC are two examples - tend to be simpler since they normally require only the largest wave speed while they can also have high resolution comparable with upwind schemes (Caleffi et al., 2007; Canestrelli et al., 2010).

In this paper we present an anti-diffusive, non-oscillatory central (*adNOC*) scheme to solve the 2D shallow water equations coupled to an erodible substrate that is straightforward, robust and accurate. The scheme is based on the well balanced scheme presented in (Zia, 2016) which is an extension of the non oscillatory central (NOC) scheme (see (Nessyahu and Tadmor, 1990; Jiang and Tadmor, 1998; Jiang et al., 1998)), which itself is a higher order extension of the classical first order centered Lax-Friedrichs scheme. The extended NOC scheme, referred as *adNOC* uses an anti-diffusive correction to reduce numerical dissipation suffered by central schemes when solving coupled systems (see (Zia, 2015) for detail). The numerical dissipation arises due to difference in characteristic time scales of the coupled systems which causes the relatively less dynamic processes to be solved with small time steps, for which NOC schemes are known to be diffusive (Kurganov and Tadmor, 2000; Huynh, 2003; Kurganov and Lin, 2007; Siviglia et al., 2013; Canestrelli and Toro, 2012; Stecca et al., 2012). Although the method presented is second-order accurate in time and space, higher order cell reconstructions could be employed, if desired, to increase accuracy (e.g., (Harten, 1983; Wang et al., 2004)). The *adNOC* scheme presented here has additional advantages over other Riemann-solver free central schemes such as the central-upwind schemes (Kurganov and Levy, 2002; Kurganov et al., 2007; Bryson et al., 2011; Bollermann et al., 2013a,b; Liu et al., 2015; Beljadid et al., 2016) and *PRICE* schemes (Canestrelli et al., 2009, 2010) as it requires the wave structure of the system only to estimate the upper bound on the time step and not to calculate fluxes. For the coupled system being solved here, the upper bound calculated with the largest wave speed of the shallow water equations is found to be sufficient for stability in almost all cases (Cordier et al. (2011)). Hence the system is solved without the Jacobian and eigen values of the sediment transport component. This provides the much needed flexibility to change the empirical relations to calculate sediment fluxes on case to case basis, without having to calculate their Jacobian.

In what follows, we present the governing equations, details of the numerical scheme (based largely on the formulation presented by (Pudasaini and Hutter, 2007) for modelling granular flows) and anti-diffusion correction, along with several computed test cases.

Governing Equations

The equations governing 2D shallow water flow coupled to an erodible substrate comprise of mass and momentum conservation equations for the water-sediment mixture and the mass conservation equations for the sediment and bed material. The equations are written as:

$$\frac{\partial h}{\partial t} + \frac{\partial(hu)}{\partial x} + \frac{\partial(hv)}{\partial y} = -\frac{\partial z}{\partial t}, \quad (1)$$

$$\frac{\partial(hu)}{\partial t} + \frac{\partial}{\partial x} \left(hu^2 + \frac{1}{2}gh^2 \right) + \frac{\partial}{\partial y} (huv) = B_x, \quad (2)$$

$$\frac{\partial(hv)}{\partial t} + \frac{\partial}{\partial x} (huv) + \frac{\partial}{\partial y} \left(hv^2 + \frac{1}{2}gh^2 \right) = B_y, \quad (3)$$

$$\frac{\partial(hc)}{\partial t} + \frac{\partial(hcu)}{\partial x} + \frac{\partial(hcv)}{\partial y} = E - D, \quad (4)$$

$$\frac{\partial z}{\partial t} + \frac{1}{1-\phi} \frac{\partial q_x}{\partial x} + \frac{1}{1-\phi} \frac{\partial q_y}{\partial y} = \frac{D-E}{1-\phi}, \quad (5)$$

where B_x and B_y are source/sink terms defined as

$$B_x = -gh \frac{\partial z}{\partial x} - ghS_{fx} - \frac{(\rho_s - \rho_w)gh^2}{2\rho} \frac{\partial c}{\partial x} + \frac{(\rho_0 - \rho)u}{\rho} \frac{\partial z}{\partial t}, \quad (6)$$

$$B_y = -gh \frac{\partial z}{\partial y} - ghS_{fy} - \frac{(\rho_s - \rho_w)gh^2}{2\rho} \frac{\partial c}{\partial y} + \frac{(\rho_0 - \rho)v}{\rho} \frac{\partial z}{\partial t}. \quad (7)$$

Similar equations have been presented by (Fagherazzi and Sun, 2003; Cao et al., 2004; Simpson and Castelltort, 2006; Xia et al., 2010; Yue et al., 2008b). In these equations, t is the time, x and y are horizontal coordinates, h is the flow depth, u and v are depth-averaged velocities in the x and y directions respectively, z is the bed elevation, c is the depth-averaged volumetric sediment concentration, g is the gravitational acceleration, S_{fx} and S_{fy} are friction slopes in the x and y directions respectively, ϕ is the bed sediment porosity, E and D are substrate entrainment and deposition fluxes across the bottom boundary of flow (representing sediment exchange between the water column and bed), $\rho = \rho_w(1-c) + \rho_sc$ is the density of the water-sediment mixture, $\rho_0 = \rho_w\phi + \rho_s(1-\phi)$ is the density of the saturated bed, ρ_s , ρ_w are the densities of water and sediment respectively and q_x , q_y are bed load fluxes in the x and y directions respectively (see table 1 for a summary of notation).

Eq. (1) and Eq. (4) represents the mass conservation for water and sediment whereas Eq. (2) and Eq. (3) represents momentum conservation in x and y directions respectively. The terms on the left side of Eq. (2) and (3) account for inertia and pressure effects in the flowing fluid. The terms B_x and B_y are the source terms which are expanded in Eq. (6) and (7) respectively. In Eq. (6) and (7), the terms from left to right, account for bed topography, friction loss, spatial variations in sediment concentration and momentum transfer between the flow and the erodible bed. The first two terms are part of the classical clear-water equations whereas the last two terms only become important in highly concentrated flows and can be neglected in situations where the sediment concentration is low. Dispersive sediment transport has been neglected in the model but can be included by adding additional diffusion terms. The sediment mass conservation represented by Eq. (4) signifies the suspended component of sediment being transported, which increases when the local erosive flux E exceeds the depositional flux D . Eq. (5) is the Exner equation (e.g. see (Paola and Voller, 2005)) which accounts for the change in the bed elevation as a result of variations in bed load fluxes q_x, q_y and the local sediment erosive and depositional fluxes.

In order to close the governing equations, it is necessary to specify additional relations for the friction slope, the substrate exchange fluxes between water and bed, and the bedload fluxes. For the friction slope, several classical equations exist, suitability of which depends on the flow conditions. In this study we have used Manning's equation to approximate friction loss for turbulent flows:

$$S_{fx} = \frac{n^2 u \sqrt{u^2 + v^2}}{h^{4/3}}, \quad S_{fy} = \frac{n^2 v \sqrt{u^2 + v^2}}{h^{4/3}}, \quad (8)$$

where n is the Manning's roughness coefficient. For quantifying entrainment and deposition fluxes, a large number of empirical relations have been proposed, a review of which can be found in (Cao and Carling, 2002). For deposition of sediment, we are using the following relation:

$$D = \omega(1 - C_a)^i C_a, \quad (9)$$

where ω is the settling velocity of a single particle in tranquil water given by:

$$\omega = \sqrt{(13.95\nu/d)^2 + 1.09\rho_s g d} - 13.95\nu/d,$$

ν is the kinematic viscosity of water, d is the grain diameter, g is the gravitational acceleration, ρ_s is the sediment particle density, C_a is the near-bed volumetric sediment concentration and i is an exponent (2 in this study). The value for C_a is computed from the relation $C_a = \alpha_c c$ where c is the depth-averaged volumetric sediment concentration and α_c is a coefficient larger than unity. In order so that the near-bed

concentration does not exceed $(1 - \phi)$ (where ϕ is the bed sediment porosity), the coefficient α_c is computed using $\alpha_c = \min(2, (1 - \phi)/c)$ (see (Cao et al., 2004)).

For calculation of erosion, we have used the following relation (see (Cao et al., 2004)):

$$E = \zeta \frac{160}{R^{0.8}} \frac{(1 - \phi)}{\theta_c} \frac{d(\theta - \theta_c)U_\infty}{h}, \quad (10)$$

where $R = d\sqrt{sgd}/\nu$, d is the sediment grain size, $s = \rho_s/\rho_w - 1$, ν is the kinematic viscosity of water, θ is Shields parameter = $u_*/(sgd)$, u_* is the friction velocity ($= \sqrt{f/8}\sqrt{u^2 + v^2}$), f is Darcy-Weisbach friction factor, θ_c is the critical value of the Shields parameter for the initiation of sediment motion below which $E = 0$, U_∞ is the free surface velocity = $7\sqrt{u^2 + v^2}/6$. Since the erosion formulation proposed in (Cao et al., 2004) approximates the total sediment flux including both suspended load and bedload, we have added a factor ζ in Eq. (10) bounded by $0 \leq \zeta \leq 1$ signifying the suspended load component of the total sediment transport. This is done due to the fact that the model has explicit bedload flux terms in the Exner equation.

Same as the erosion and deposition, there is a large number of empirical formulations present in literature to approximate the bedload flux (e.g. see (Yang, 2006) for a detailed review). In this study we use the shear stress free formulation discussed by Grass (Grass, 1981) given by:

$$q_x = Au(\sqrt{u^2 + v^2})^{b-1}, \quad q_y = Av(\sqrt{u^2 + v^2})^{b-1}, \quad (11)$$

where A is a constant signifying the interaction of the sediment with the flow and b is an exponent ($1 \leq b \leq 4$). Although being fairly basic, as it does not assume any critical threshold velocity to initiate bedload transport, the Grass formulation has been used by many previous studies (e.g. (Liu et al., 2008; Benkhaldoun et al., 2010; Črnjarić-Žic et al., 2004; Siviglia et al., 2013)).

There are several advantages of the sediment transport formulation such as that presented here (see also (Capart and Young, 1998; Cao et al., 2004; Simpson and Castelltort, 2006)). First, the evaluation of entrainment and deposition is done independently of each other. This is not only convenient but it makes good sense given that erosion and sedimentation are governed by completely different physics. In contrast to the sediment capacity approach where the change in local bed morphology is evaluated by considering whether the sediment discharge is greater or less than the sediment transport capacity, the change in bed morphology is evaluated by taking the difference between the local erosion and deposition fluxes. Thus, there is no need for assumptions concerning whether sediment transport is supply-limited or transport-limited. Second, the distinction between the bedload and suspended load is made, which is necessary because the suspended load and bedload are governed by different physics. For example, bedload transport is affected by

bottom slope while suspended sediment load is not. Moreover, the suspended sediment is transported with the velocity of the flow while bedload is usually transported at a slower rate. Finally, because an attempt is made to clearly separate the governing equations from the empirical relations, the formulae for calculation of the substrate exchange and bedload fluxes can readily be modified to incorporate new transport models or to study different applications. The advantage of such formulation is fully availed by the central scheme presented here. For the upwind schemes, in comparison, a change in the empirical formulation changing the wavestructure of the system will require analytical relations for the new wave speeds or their numerical calculation which is computationally costly.

NOC Numerical Scheme

The numerical scheme utilized to solve the equations is based on the non-oscillatory central (NOC) scheme developed by (Nessyahu and Tadmor, 1990) (see also (Jiang et al., 1998; Jiang and Tadmor, 1998)). The scheme uses a two step predictor-corrector procedure. The first step involves first order prediction of the grid values according to non-oscillatory reconstructions from given cell averages while the second step involves staggered averaging to determine the full evolution of these averages. Below, we present details, based largely on the formulation presented by (Pudasaini and Hutter, 2007), of how this scheme can be used to solve the two dimensional shallow water equations coupled to a mobile substrate.

For the purposes of obtaining a numerical solution we write the governing equations in the vector form as follows:

$$\frac{\partial W}{\partial t} + \frac{\partial F}{\partial x} + \frac{\partial G}{\partial y} = S, \quad (12)$$

where W is the solution vector defined as:

$$W = \begin{bmatrix} h \\ hu \\ hv \\ hc \\ z \end{bmatrix}, \quad (13)$$

F and G are flux vectors defined as:

$$F = \begin{bmatrix} hu \\ hu^2 + \frac{1}{2}gh^2 \\ huv \\ huc \\ \frac{1}{1-\phi}q_x \end{bmatrix}, \quad (14)$$

$$G = \begin{bmatrix} hv \\ huv \\ hv^2 + \frac{1}{2}gh^2 \\ hvc \\ \frac{1}{1-\phi}q_y \end{bmatrix}, \quad (15)$$

and S is the source vector defined by:

$$S = \begin{bmatrix} -\frac{\partial z}{\partial t} \\ B_x \\ B_y \\ E - D \\ \frac{D-E}{1-\phi} \end{bmatrix}. \quad (16)$$

We begin by dividing the two dimensional spatial domain into rectangular cells (see Fig. 1). Let $C_{p,q}$ denote the cell that covers the region $|x - x_p| \leq \frac{\Delta x}{2}, |y - y_q| \leq \frac{\Delta y}{2}$, where p and q are integer node indices and Δx and Δy are grid spacings in the x and y directions respectively. For the development below, we note that the cell $C_{p+1/2,q+1/2}$ consists of the overlap between four intersecting cells $C_{p,q}, C_{p+1,q}, C_{p+1,q+1}, C_{p,q+1}$, denoted $C^{SW}, C^{SE}, C^{NE}, C^{NW}$ (see Figure 1). Let $\overline{W}_{p,q}^n$ denote the cell average over the cell at time t^n . The solution can be reconstructed in space linearly over the cell from the average by:

$$W_{p,q}(x, y, t^n) = \overline{W}_{p,q}^n + \sigma_{p,q}^x(x - x_p) + \sigma_{p,q}^y(y - y_q), \quad (x, y) \in C_{p,q}, \quad (17)$$

where σ^x and σ^y are the discrete slopes of W in the x and y directions, respectively. This reconstruction is used to achieve second-order accuracy in space. Second-order temporal accuracy is achieved by using a predictor-corrector procedure in which the solution is first evaluated at the half time step in the predictor

step. Linear reconstruction is also used for reconstruction in time:

$$\overline{W}_{p,q}^{n+1/2} = \overline{W}_{p,q}^n + \frac{\Delta t}{2} \left(\frac{\partial W}{\partial t} \right)^n,$$

where $\left(\frac{\partial W}{\partial t} \right)^n$ is calculated using the conservation law (i.e., Eq. 12):

$$\left(\frac{\partial W}{\partial t} \right)^n = - \left(\frac{\partial F(W)}{\partial x} \right)^n - \left(\frac{\partial G(W)}{\partial y} \right)^n + S(\overline{W}^n). \quad (18)$$

Thus the predictor step is given by:

$$\overline{W}_{p,q}^{n+1/2} = \overline{W}_{p,q}^n - \frac{\Delta t}{2} (\sigma^F)_{p,q}^n - \frac{\Delta t}{2} (\sigma^G)_{p,q}^n + \frac{\Delta t}{2} S(\overline{W}_{p,q}^n), \quad (19)$$

where σ^F and σ^G are one-dimensional discrete slopes of the fluxes F and G in the x and y directions, respectively.

To calculate the second order solution for the conservation law given by Eq. (12), we integrate it over the cell $C_{p+\frac{1}{2},q+\frac{1}{2}}$ and time period $[t^n, t^{n+1}]$. The staggered average over $C_{p+\frac{1}{2},q+\frac{1}{2}}$ is given by:

$$\begin{aligned} \overline{W}_{p+1/2,q+1/2}^{n+1} &= \frac{1}{\Delta x \Delta y} \int_{x_p}^{x_{p+1}} \int_{y_q}^{y_{q+1}} W(x, y, t^n) dx dy - \frac{1}{\Delta x \Delta y} \int_{t^n}^{t^{n+1}} \int_{y_q}^{y_{q+1}} (F(x_{p+1}, y, t) - F(x_p, y, t)) dy dt \\ &\quad - \frac{1}{\Delta x \Delta y} \int_{t^n}^{t^{n+1}} \int_{x_p}^{x_{p+1}} (G(x, y_{q+1}, t) - G(x, y_q, t)) dx dt + \frac{1}{\Delta x \Delta y} \int_{t^n}^{t^{n+1}} \int_{x_p}^{x_{p+1}} \int_{y_q}^{y_{q+1}} S(x, y, t) dx dy dt. \quad (20) \end{aligned}$$

We now consider how to separately compute each of the terms in this equation (20). The first term on the right hand side can be split into four parts representing the individual contributions from the four adjacent intersecting cells on the staggered grid (see Fig. 1):

$$\begin{aligned} \int_{x_p}^{x_{p+1}} \int_{y_q}^{y_{q+1}} W(x, y, t^n) dx dy &= \int \int_{C^{SW}} W(x, y, t^n) dx dy + \int \int_{C^{SE}} W(x, y, t^n) dx dy \\ &\quad + \int \int_{C^{NE}} W(x, y, t^n) dx dy + \int \int_{C^{NW}} W(x, y, t^n) dx dy. \quad (21) \end{aligned}$$

To evaluate this integral, we begin by integrating the reconstructing polynomial (Eq. 17) over the sub-cell C^{SW} . The integral is given by:

$$\int \int_{C^{SW}} W(x, y, t^n) = \int_{x_p}^{x_{p+1/2}} \int_{y_q}^{y_{q+1/2}} (\overline{W}_{p,q}^n + \sigma_{p,q}^x(x - x_p) + \sigma_{p,q}^y(y - y_q)) dx dy.$$

Calculating the definite integral and dividing by $\Delta x \Delta y$ to get the cell average:

$$\frac{1}{\Delta x \Delta y} \int \int_{C^{SW}} W(x, y, t^n) = \frac{1}{4} \overline{W}_{p,q}^n + \frac{\Delta x}{16} \sigma_{p,q}^x + \frac{\Delta y}{16} \sigma_{p,q}^y.$$

The other terms in Eq. (21) can be calculated by the same procedure, leading to:

$$\frac{1}{\Delta x \Delta y} \int \int_{C^{NW}} W(x, y, t^n) = \frac{1}{4} \overline{W}_{p,q+1}^n + \frac{\Delta x}{16} \sigma_{p,q+1}^x - \frac{\Delta y}{16} \sigma_{p,q+1}^y,$$

$$\frac{1}{\Delta x \Delta y} \int \int_{C^{NE}} W(x, y, t^n) = \frac{1}{4} \overline{W}_{p+1,q+1}^n - \frac{\Delta x}{16} \sigma_{p+1,q+1}^x - \frac{\Delta y}{16} \sigma_{p+1,q+1}^y,$$

$$\frac{1}{\Delta x \Delta y} \int \int_{C^{SE}} W(x, y, t^n) = \frac{1}{4} \overline{W}_{p+1,q}^n - \frac{\Delta x}{16} \sigma_{p+1,q}^x + \frac{\Delta y}{16} \sigma_{p+1,q}^y.$$

Next, we compute the second and third terms in Eq. (20), i.e. the integral of fluxes through the four edges of each cell. The fluxes at the northern and southern edges are associated with the flux function G whereas the fluxes at the eastern and western edges are associated with the flux function F . To calculate the integral, we use the midpoint quadrature rule. For example, the flux integral at the western edge is given by:

$$\begin{aligned} \frac{1}{\Delta x \Delta y} \int_{t^n}^{t^{n+1}} \int_{y^q}^{y^{q+1}} F(x_p, y, t) dy dt &= \frac{\Delta t}{2 \Delta x} (F(x_p, y_q, t^{n+1/2}) + F(x_p, y_{q+1}, t^{n+1/2})) \\ &= \frac{\Delta t}{2 \Delta x} (F(\overline{W}_{p,q}^{n+1/2}) + F(\overline{W}_{p,q+1}^{n+1/2})). \end{aligned}$$

Similarly, the integral of fluxes respectively through the eastern, southern and northern edges of the cell are:

$$\frac{1}{\Delta x \Delta y} \int_{t^n}^{t^{n+1}} \int_{y^q}^{y^{q+1}} F(x_{p+1}, y, t) dy dt = \frac{\Delta t}{2 \Delta x} (F(\overline{W}_{p+1,q}^{n+1/2}) + F(\overline{W}_{p+1,q+1}^{n+1/2})),$$

$$\frac{1}{\Delta x \Delta y} \int_{t^n}^{t^{n+1}} \int_{x^p}^{x^{p+1}} G(x, y_q, t) dx dt = \frac{\Delta t}{2 \Delta y} (G(\overline{W}_{p,q}^{n+1/2}) + G(\overline{W}_{p+1,q}^{n+1/2})),$$

$$\frac{1}{\Delta x \Delta y} \int_{t^n}^{t^{n+1}} \int_{x^p}^{x^{p+1}} G(x, y_{q+1}, t) dx dt = \frac{\Delta t}{2 \Delta y} (G(\overline{W}_{p,q+1}^{n+1/2}) + G(\overline{W}_{p+1,q+1}^{n+1/2})).$$

Note that the solution at half time step is evaluated in the predictor step (Eq. 19). Finally, we compute

the last remaining term in Eq. (20) i.e. the integration of the source term. The integral is computed by adding up contributions from the four neighbouring cells i.e. the sub-cells SC^{SW} , SC^{SE} , SC^{NE} and SC^{NW} . The source is evaluated at the centers of the contributing sub-cells and the average of the four is taken for calculation of the predictor step:

$$\begin{aligned} \frac{1}{\Delta x \Delta y} \int_{t^n}^{t^{n+1}} \int_{x_p}^{x_{p+1}} \int_{y_q}^{y_{q+1}} S(x, y, t) dx dy dt &= \frac{\Delta t}{4} \{S(\overline{W}_{p+1/4, q+1/4}^{n+1/2}) + S(\overline{W}_{p+3/4, q+1/4}^{n+1/2}) \\ &+ S(\overline{W}_{p+1/4, q+3/4}^{n+1/2}) + S(\overline{W}_{p+3/4, q+3/4}^{n+1/2})\}. \end{aligned}$$

The value of the solution average $\overline{W}^{n+1/2}$ at the sub-cells centers (represented by \blacksquare in Fig. 1) are computed by utilizing Taylor series expansions:

$$\overline{W}_{p+1/4, q+1/4}^{n+1/2} = \overline{W}_{p, q}^{n+1/2} + \frac{\Delta x}{4} (\sigma^x)_{p, q}^n + \frac{\Delta y}{4} (\sigma^y)_{p, q}^n,$$

$$\overline{W}_{p+3/4, q+1/4}^{n+1/2} = \overline{W}_{p+1, q}^{n+1/2} - \frac{\Delta x}{4} (\sigma^x)_{p+1, q}^n + \frac{\Delta y}{4} (\sigma^y)_{p+1, q}^n,$$

$$\overline{W}_{p+3/4, q+3/4}^{n+1/2} = \overline{W}_{p+1, q+1}^{n+1/2} - \frac{\Delta x}{4} (\sigma^x)_{p+1, q+1}^n - \frac{\Delta y}{4} (\sigma^y)_{p+1, q+1}^n,$$

$$\overline{W}_{p+1/4, q+3/4}^{n+1/2} = \overline{W}_{p, q+1}^{n+1/2} + \frac{\Delta x}{4} (\sigma^x)_{p, q+1}^n - \frac{\Delta y}{4} (\sigma^y)_{p, q+1}^n.$$

Collecting all the terms in the Eq. (20) results in the standard second-order, non-oscillatory central scheme given by:

$$\begin{aligned} \overline{W}_{p+1/2, q+1/2}^{n+1} &= \frac{1}{4} \{ \overline{W}_{p, q}^n + \overline{W}_{p+1, q}^n + \overline{W}_{p, q+1}^n + \overline{W}_{p+1, q+1}^n \} \\ &+ \frac{\Delta x}{16} \{ \sigma_{p, q}^x - \sigma_{p+1, q}^x - \sigma_{p+1, q+1}^x + \sigma_{p, q+1}^x \} \\ &+ \frac{\Delta y}{16} \{ \sigma_{p, q}^y + \sigma_{p+1, q}^y - \sigma_{p+1, q+1}^y - \sigma_{p, q+1}^y \} \\ &- \frac{\Delta t}{2\Delta x} \{ F(\overline{W}_{p+1, q}^{n+1/2}) + F(\overline{W}_{p+1, q+1}^{n+1/2}) - F(\overline{W}_{p, q}^{n+1/2}) - F(\overline{W}_{p, q+1}^{n+1/2}) \} \end{aligned}$$

$$-\frac{\Delta t}{2\Delta y}\{G(\overline{W}_{p,q+1}^{n+1/2}) + G(\overline{W}_{p+1,q+1}^{n+1/2}) - G(\overline{W}_{p,q}^{n+1/2}) - G(\overline{W}_{p+1,q}^{n+1/2})\}$$

$$+\frac{\Delta t}{4}\{S(\overline{W}_{p+1/4,q+1/4}^{n+1/2}) + S(\overline{W}_{p+3/4,q+1/4}^{n+1/2}) + S(\overline{W}_{p+3/4,q+3/4}^{n+1/2}) + S(\overline{W}_{p+1/4,q+3/4}^{n+1/2})\}. \quad (22)$$

It is important to remember that while the high order nature of the scheme assures that shocks and discontinuities are captured, this comes at the expense of spurious oscillations. To avoid these oscillations, NOC scheme uses the well-known Total Variation Diminishing (TVD) concept (see (Harten, 1983)) by calculating the slopes σ^x , σ^y and the flux slopes σ^F , σ^G using limiters (e.g. *min-mod*, *superbee*, etc.). In this study, we have used the *min-mod* limiter given by:

$$\text{minmod}\{r_1, r_2\} = \frac{1}{2}[\text{sgn}(r_1) + \text{sgn}(r_2)].\text{Min}(|r_1|, |r_2|),$$

where r_1 and r_2 are the slopes at successive positions on the solution mesh in any given direction.

Because the numerical scheme presented is entirely explicit, the maximum allowable time step for stability is constrained by the Courant-Friedrichs-Lewy condition. In this study we compute the time step dynamically according to the condition:

$$\Delta t = \min(\Delta x Cn/V_{max}, \Delta y Cn/V_{max}),$$

where Cn is the Courant number and V_{max} is the maximum wave speed. The Courant number must have a value of unity or less in order for the scheme to be numerically stable. For the maximum wave speed, we are using the largest eigen value of the shallow water equations:

$$V_{max} = \max(|u - \sqrt{gh}|, |u + \sqrt{gh}|, |v - \sqrt{gh}|, |v + \sqrt{gh}|).$$

As noted by Cordier et al. (2011), estimating maximum wave speed of the coupled shallow water/sediment transport system with the largest eigen value of the shallow water equation can be problematic for splitting schemes, but is sufficient for Lax-Friedrich scheme based central schemes. Hence for the *adNOC* scheme, the solution is evaluated without any knowledge of the wave structure of the sediment transport system.

Anti-diffusion correction

Despite the advantages of simplicity and universality, there are certain cases where use of the standard central scheme described above becomes unfeasible. Central schemes are known to be excessively diffusive, especially

when small time steps are used (Kurganov and Tadmor, 2000; Huynh, 2003; Kurganov and Lin, 2007; Siviglia et al., 2013; Canestrelli and Toro, 2012). This problem of excessive numerical dissipation becomes highly significant in the case of coupled morphodynamic equations due to the difference in characteristic time scales. As discussed before, for the coupled system of equations presented above, the time step is controlled by the more dynamic component of the system i.e. shallow water equations. This time step is very small for the relatively passive process of bed evolution and causes excessive smearing of the bed topography as the solution evolves. In an attempt to remedy this, we present an anti-diffusive, non-oscillatory (*adNOC*) scheme (see also (Zia, 2015)) that has reduced diffusion and is suitable for coupled systems such as the morphodynamic equations presented in this study.

Consider the NOC scheme in one dimension:

$$\begin{aligned} \bar{u}_j^{n+1} = & \frac{1}{2}(\bar{u}_{j+1/2}^n + \bar{u}_{j-1/2}^n) + \frac{\Delta x}{8}(\sigma_{j-1/2}^n - \sigma_{j+1/2}^n) \\ & - \lambda(f_{j+1/2}^{n+1/2} - f_{j-1/2}^{n+1/2}) + \frac{\Delta t}{2}(s_{j+1/4}^{n+1/2} + s_{j-1/4}^{n+1/2}). \end{aligned} \quad (23)$$

To demonstrate the anti-diffusive correction, let's assume that the system is at steady state and there is no source. This will remove the third and fourth term in Eq. (23) leaving just the first two terms:

$$\bar{u}_j^{n+1} = \frac{1}{2}(\bar{u}_{j+1/2}^n + \bar{u}_{j-1/2}^n) + \frac{\Delta x}{8}(\sigma_{j-1/2}^n - \sigma_{j+1/2}^n). \quad (24)$$

By substituting

$$\bar{u}_{j-1/2}^n = \frac{1}{2}(\bar{u}_{j-1}^{n-1} + \bar{u}_j^{n-1}) + \frac{\Delta x}{8}(\sigma_{j-1}^{n-1} - \sigma_j^{n-1})$$

and

$$\bar{u}_{j+1/2}^n = \frac{1}{2}(\bar{u}_j^{n-1} + \bar{u}_{j+1}^{n-1}) + \frac{\Delta x}{8}(\sigma_j^{n-1} - \sigma_{j+1}^{n-1})$$

into Eq. (24), one obtains

$$\bar{u}_j^{n+1} = \bar{u}_j^{n-1} + \frac{1}{4}(\bar{u}_{j-1}^{n-1} - 2\bar{u}_j^{n-1} + \bar{u}_{j+1}^{n-1}) + \frac{\Delta x}{8}(\sigma_{j-1}^{n-1} - \sigma_{j+1}^{n-1}) + \frac{\Delta x}{8}(\sigma_{j-1/2}^n - \sigma_{j+1/2}^n). \quad (25)$$

The second term on the right hand side of Eq. (25) is the finite difference approximation for a diffusive term (ie., $\frac{1}{4}(\bar{u}_{j-1}^{n-1} - 2\bar{u}_j^{n-1} + \bar{u}_{j+1}^{n-1}) \approx \frac{(\Delta x)^2}{4} \frac{\partial^2 u}{\partial x^2}$), which shows the origin of numerical dissipation in this scheme. Notice that the diffusion term is applied each time a time step is taken. This means that for fixed time period, more time steps will introduce more numerical dissipation in the solution. This dissipation, however, can be mitigated or removed entirely by carefully choosing the finite difference approximations of the slopes

present in the equation (see (Zia, 2015) for detail). Substituting

$$\sigma_{j-1}^{n-1} = \sigma_{j-1/2}^n = \frac{\bar{u}_j^{n-1} - \bar{u}_{j-1}^{n-1}}{\Delta x} \quad \text{and} \quad \sigma_{j+1}^{n-1} = \sigma_{j+1/2}^n = \frac{\bar{u}_{j+1}^{n-1} - \bar{u}_j^{n-1}}{\Delta x}$$

into Eq. (25) results in:

$$\bar{u}_j^{n+1} = \bar{u}_j^{n-1}.$$

Thus, the solution is exactly maintained. The Anti-diffusive, Non-oscillatory Central difference (*adNOC*) scheme is given by rewriting the NOC scheme with the anti-diffusive slopes:

$$\begin{aligned} \bar{u}_{j+1/2}^{n+1} = & \frac{1}{2}(\hat{u}_{j+1}^n + \hat{u}_j^n) + \frac{\Delta x}{8}(1 - \varepsilon)(\sigma_j^n - \sigma_{j+1}^n) - \frac{\varepsilon}{4}(\bar{u}_{j+3/2}^{n-1} - 2\bar{u}_{j+1/2}^{n-1} + \bar{u}_{j-1/2}^{n-1}) \\ & - \lambda(f_{j+1}^{n+1/2} - f_j^{n+1/2}) + \frac{\Delta t}{2}(s_{j+1/4}^{n+1/2} + s_{j+3/4}^{n+1/2}). \end{aligned} \quad (26)$$

where \hat{u} is the cell average evaluated without the anti-diffusion correction i.e. the third term in the right hand side of (26). The new parameter ε is the factor ($0 \leq \varepsilon \leq 1$) signifying the strength of the anti-diffusive slopes. A value of 1 for ε means that only anti-diffusive slopes are used in calculation of reconstructions while a value of 0 means that the standard NOC scheme is used. Following this discussion along with the discussion in the previous section, the *adNOC* scheme for the system (12-16) is given by:

$$\begin{aligned} \bar{W}_{p+1/2, q+1/2}^{n+1} = & \frac{1}{4}\{\hat{W}_{p,q}^n + \hat{W}_{p+1,q}^n + \hat{W}_{p,q+1}^n + \hat{W}_{p+1,q+1}^n\} \\ & + \frac{\Delta x}{16}(1 - \varepsilon)\{\sigma_{p,q}^x - \sigma_{p+1,q}^x - \sigma_{p+1,q+1}^x + \sigma_{p,q+1}^x\} \\ & + \frac{\Delta y}{16}(1 - \varepsilon)\{\sigma_{p,q}^y + \sigma_{p+1,q}^y - \sigma_{p+1,q+1}^y - \sigma_{p,q+1}^y\} - \varepsilon\Psi \\ & - \frac{\Delta t}{2\Delta x}\{F(\bar{W}_{p+1,q}^{n+1/2}) + F(\bar{W}_{p+1,q+1}^{n+1/2}) - F(\bar{W}_{p,q}^{n+1/2}) - F(\bar{W}_{p,q+1}^{n+1/2})\} \\ & - \frac{\Delta t}{2\Delta y}\{G(\bar{W}_{p,q+1}^{n+1/2}) + G(\bar{W}_{p+1,q+1}^{n+1/2}) - G(\bar{W}_{p,q}^{n+1/2}) - G(\bar{W}_{p+1,q}^{n+1/2})\} \\ & + \frac{\Delta t}{4}\{S(\bar{W}_{p+1/4, q+1/4}^{n+1/2}) + S(\bar{W}_{p+3/4, q+1/4}^{n+1/2}) + S(\bar{W}_{p+3/4, q+3/4}^{n+1/2}) + S(\bar{W}_{p+1/4, q+3/4}^{n+1/2})\}. \end{aligned}$$

where Ψ is the 2D anti-diffusive component of the slopes given by:

$$\begin{aligned} \Psi = & -\frac{3}{4}\overline{W}_{p+1/2,q+1/2}^{n-1} \\ & +\frac{1}{8}(\overline{W}_{p+1/2,q-1/2}^{n-1} + \overline{W}_{p+1/2,q+3/2}^{n-1} + \overline{W}_{p-1/2,q+1/2}^{n-1} + \overline{W}_{p+3/2,q+1/2}^{n-1}) \\ & +\frac{1}{16}(\overline{W}_{p-1/2,q-1/2}^{n-1} + \overline{W}_{p+3/2,q-1/2}^{n-1} + \overline{W}_{p-1/2,q+3/2}^{n-1} + \overline{W}_{p+3/2,q+3/2}^{n-1}) \end{aligned} \quad (27)$$

More details on the *adNOC* scheme including several test cases and discussion on the stability can be seen in (Zia, 2015). The proof of the one dimensional anti-diffusive scheme being well-balanced can be seen in (Zia, 2016), which can be straightforwardly extended to two dimensions.

Results

In this section we demonstrate the ability of the *adNOC* scheme to solve the shallow water equations over a mobile substrate by studying several different test cases.

Dam Break over erodible bed in one dimension

The performance of the numerical scheme for the solution of the coupled morphodynamic model is assessed by considering a mobile bed, dam break problem. The numerical experiment has been investigated previously by (Cao et al., 2004) and (Simpson and Castelltort, 2006) where the solutions were obtained with upwind methods based on approximate Riemann solvers. The model setup consists of a 50 *km* long, horizontal, one-dimensional channel with a dam located at 25 *km* separating two initially stagnant bodies of water with depths of 40 *m* and 2 *m*. The dam is breached instantaneously which results in a sharp shock wave downstream of the initial dam along with a smooth rarefaction wave upstream within the reservoir. These waves cause the base to deform in response to erosion and sedimentation. The Values used for ε along with other parameters are presented in Table 2. We set $\zeta = 1$ and $A = 0$, to use the same empirical formulations as in the previous studies to compare the numerical schemes. Fig. 2 shows the wave height, bed elevation and sediment concentration near the location of the failed dam after 60 seconds. Results show the development of a heavily concentrated, eroding wavefront which forms at the location of the failed dam and diminishes as it propagates downstream. A hydraulic jump is formed near the previous dam site due to rapid bed erosion that reaches a height of approximately 5 meters. It can be seen that the sediment transport and bed friction have a strong influence on the wave height in the dam break scenario. Results presented in Fig. 2 agree with those computed by (Cao et al., 2004) and (Simpson and Castelltort, 2006) using Riemann-based solvers.

Dam Break over erodible bed in two dimensions

The second test considered is the two dimensional dam break problem introduced by Cao et al. (Cao et al., 2010), which was designed to reproduce results of a flume experiment. The experiment consists of a flume, 3.6 *m* wide and 36 *m* long, containing an erodible bed made of uniform coarse grained sand. A one meter wide gate centered across the middle of the flume is located about 12 *m* from the upstream end of the flume. The gate initially separates a 0.47 *m* deep upstream water reservoir from an initially dry bed below the gate. The bed material consists of 85 *mm* deep, fully saturated sand with grain size of 1.61 *mm* and a Manning’s roughness coefficient of 0.0165. A complete list of parameters is provided in table 2.

For the numerical simulation, the boundary conditions are closed wall along the lateral and upstream boundaries and a transmissive boundary at the downstream end. The spatial domain was discretized with 300 cells in the long direction and 100 cells across the flume. The Courant number was set to 0.4. The bedload flux was calculated using $A = 0.0001$, $b = 3$ and the coefficient $\zeta = 0.01$, meaning that sediment transport is dominated by the bedload.

Fig. 3 shows the portion of bed topography downstream of the gate 20 seconds after the breach of the dam computed with the new adNOC scheme (3a), along with a comparison with the original laboratory experiment (3b) and numerical results computed by (Cao et al., 2010) with a Riemann based upwind scheme (3c). The dam break is seen cause scouring close to the gate, while a cone shaped dune is deposited further downstream. The *adNOC* scheme produces results consistent with both the laboratory experiment and the Riemann-based numerical solution.

Evolution of a conical dune

In this test, we investigate the flow of water over a mobile sand dune. The test was proposed by Hudson and Sweby (Hudson and Sweby, 2005) and has been used by many other studies to assess the performance of two dimensional morphodynamic models (e.g. (Siviglia et al., 2013; Benkhaldoun et al., 2010; D1 et al., 2009; Canestrelli et al., 2010)). The experiment is a good test of the stability and diffusivity of the numerical scheme as it evaluates very slow evolving bed topography over a long period of time. The test consists of a 1000×1000 *m* square domain with an initial bathymetry given by:

$$z(x, y, 0) = \begin{cases} 0.1 + \sin^2\left(\frac{\pi(x-300)}{200}\right) \sin^2\left(\frac{\pi(y-400)}{200}\right) & \text{if } x \in [300, 500], y \in [400, 600] \\ 0.1 & \text{if } otherwise \end{cases}$$

The boundary conditions are a constant unit discharge of $10 \text{ m}^2/\text{s}$ on the inflow upstream and outflow downstream boundaries. The sides are reflective, free slip boundaries. The initial flow conditions are calculated by applying an initial water level ($h + z$) of 10.1 meters over the whole of the domain and a boundary flux of $10 \text{ m}^2/\text{s}$ and $0 \text{ m}^2/\text{s}$ in the x and y directions respectively, and by allowing the solution to evolve under fixed base conditions until a steady state is achieved. This steady state is then taken as time zero for the movable bed experiment and the deformation of the sand dune is tracked. We use sediment transport parameters that imply loose coupling between the bedload and flow. The parameter A in the Grass formula is set to 0.001 and the exponent b is chosen to be 3. In order to compare our results with other published studies, suspended load is neglected (i.e., $\zeta = 0$). The parameter ε is taken as 0.3 for the shallow water system and 1 for the Exner equation. We use 200 cells in each direction and a Courant number of 0.5. The values used for all the parameters can be seen in Table 2.

Numerical results, presented in Fig. 4, show that a star shaped bedform emerges as the result of coupling between sediment transport and the flowing water. Results computed with the adNOC scheme (4) are similar to the results published by previous studies ((Siviglia et al., 2013; Benkhaldoun et al., 2010; Di et al., 2009)). De Vriend, in ((De Vriend, 1987)), derived an analytical expression to predict the spread angle of the star shaped pattern under weak flow conditions ($A < 0.01$) given by:

$$\theta = \arctan\left(\frac{3\sqrt{3}(m-1)}{9m-1}\right)$$

In this case for $A = 0.001$ and $b = 3$, the spread angle is predicted to be $\theta = 21.787^\circ$, which agrees with our numerical results (24.4°).

Stratigraphic development of a one dimensional sediment wedge

This test is based on a aggradation flume experiment performed by Postma et. al (Postma et al., 2008). The setup consists of an initially horizontal 4.5 m long, 0.11 m wide duct, into which sediment and water are slowly fed. The water discharge and sediment supply at the upstream boundary are $350 \text{ dm}^3\text{h}^{-1}$ and $1.7 \text{ dm}^3\text{h}^{-1}$, respectively. The sediment has a mean grain size of $250 \text{ }\mu\text{m}$ and D_{90} of $700 \text{ }\mu\text{m}$. In the experiments performed by Postma et al. (Postma et al., 2008), elevation profiles were measured every hour for the first 44 hours (Fig. 5a).

We simulate the experiment data using a one dimensional version of the model, which is acceptable because the width of the flume is far smaller than its length. Otherwise, the setup and boundary conditions correspond as closely as possible to those used in the laboratory experiment. The domain is divided into 200 cells and the Courant number is set to 0.5. The numerical experiment is done with only bedload sediment

transport, i.e. $\zeta = 0$. This makes sense because the water discharge is fairly low and suspended transport is unlikely to occur. The upstream boundary conditions consist of a fixed water depth (0.01 m) and velocity (0.0883 m/s). The downstream boundary is set to be transmissive outflow with the fixed water depth (0.01 m). The parameter values for the Grass bedload model are $A = 0.04$ and $b = 4$ and a Manning roughness coefficient of 0.082 is used for calculation of the friction slope. The rest of the parameter values are shown in Table 2. The numerical results presented in Fig. 5, show the formation of a sand wedge which propagates progressively downstream with time until the lower boundary is reached when a steady state bed profile is achieved. The final equilibrium slope of the numerical experiments (0.0284) agrees well with that determined from the flume experiments (i.e., 0.02857) and from a simple analytical model (0.026).

Two dimensional flume experiment

The final experiment is done with the aim of demonstrating the robustness of the *adNOC* scheme for simulating complex flows under near steady state flow conditions. The experiment consists of a fixed base flume with the dimensions of 100 m x 10 m and an initial slope of 0.001. Sediment and water are fed into the flume through a 3 m wide inlet centered along the middle of the flume at the upstream boundary. Initial water depth is set as 0.2 m throughout the flume. The water at the inlet has a flux of 0.072 m³/s and a velocity of 0.36 m/s. The lower outflow boundary is set as transmissive with the fixed water depth of 0.2 m while the lateral boundaries are reflective. The sediment and water mixture fed at the inlet has a volumetric concentration of 1% and an additional sediment flux of 0.003 m³/s is added into the flume in the form of bedload flux. The sediment is assumed to have a grain size of 1 mm (course sand) and a Manning roughness coefficient of 0.033. The parameters values used in the experiment are provided in Table 2. We have used ζ as 0.5 and values of $A = 0.001$ and $b = 3$ are used to calculate the bedload flux with the Grass formulation. The numerical calculation presented was performed using 200×30 cells and a Courant number of 0.45.

Fig. 6 shows the calculated bed topography at various moments in time. The results show the formation of complex, dynamic bed forms due to the strong coupling between the flowing water and sediment transport. These bedforms are entirely below water. Though it is difficult and beyond the scope of this work to compare the results directly with either experimental or natural data, the results show features (e.g., bar formation, channel avulsion, channel splitting) commonly observed in nature (e.g. (Smith, 1974; Field, 2001; Kleinhans et al., 2013)). Importantly, the results illustrate the ability of the *adNOC* scheme to effectively resolve complex interactions between flow and evolution of the underlying topography.

Conclusion

A well-balanced, Anti-diffusive Non-Oscillatory Central Differencing (adNOC) scheme is presented to solve the shallow water equations coupled to substrate erosion and sediment transport in two dimensions. The scheme is Riemann solver free and simple to implement. The complete wave structure of the system is not required and only the largest wave speed is used to determine the upper bound on the time step (notably, not to calculate fluxes). This means that the solution can be evaluated without any knowledge of the wave structure of the sediment transport system and the empirical relations for erosional/depositional and bedload fluxes can easily be changed, making it especially suitable for the solution of coupled hydrodynamic/sediment transport models.

A detailed derivation of the non oscillatory second order scheme is presented demonstrating its simplicity. The cause of the commonly suffered numerical dissipation by central schemes is discussed and a correction is proposed. A range of numerical results are presented and compared with previously published numerical solutions or with laboratory experiments. The test cases include highly dynamic one and two dimensional dam break experiments and relatively slow evolving conical dune and stratigraphic development of a sediment wedge. Simulation of a two dimensional flume experiment is also performed. Comparison with published results and laboratory experiments show that the scheme is accurate and robust, suggesting that it has considerable promise to be used to study a wide range of problems where flow and substrate evolution are coupled.

Notation

The following symbols are used in this paper:

- A = coefficient in Grass formula;
- b = exponent in Grass formula;
- c = depth-averaged volumetric sediment concentration;
- C_a = near-bed volumetric sediment concentration;
- Cn = courant number;
- D = substrate deposition flux (m/s);
- d = grain diameter (m);
- E = substrate erosion flux (m/s);
- f = Darcy-Weisbach friction factor;
- g = gravitational acceleration (m/s^2);

h	=	flow depth (m);
i	=	exponent in deposition equation;
m	=	meter(s);
n	=	Manning's roughness coefficient;
s	=	submerged specific gravity of sediment;
S_{fx}	=	friction slope in x direction;
S_{fy}	=	friction slope in y direction;
t	=	time (s);
u	=	depth-averaged velocity in x direction (m/s);
u_c	=	threshold entrainment flow velocity (m/s);
u_*	=	friction velocity (m/s);
U_∞	=	free surface velocity (m/s);
v	=	depth-averaged velocity in y direction (m/s);
z	=	bed elevation (m);
α_c	=	concentration coefficient;
β	=	entrainment coefficient;
ε	=	coefficient specifying the strength of anti-diffusive slopes;
θ	=	Shield's parameter;
θ_c	=	critical value of Shield's parameter;
ν	=	kinematic viscosity of water (m^2/s);
ρ	=	density of water-sediment mixture (kg/m^3);
ρ_w	=	density of water (kg/m^3);
ρ_s	=	density of sediment (kg/m^3);
ρ_0	=	density of saturated bed (kg/m^3);
σ^x	=	discrete slope in x direction;
σ^y	=	discrete slope in y direction;
ϕ	=	bed sediment porosity;
ω	=	settling velocity of a single particle in tranquil water (m/s);
ζ	=	coefficient in erosion formula;

Table 1: List of notation used, with units in brackets where applicable.

References

- Audusse, E. and Bristeau, M.-O. (2005). A well-balanced positivity preserving “second-order” scheme for shallow water flows on unstructured meshes. *Journal of Computational Physics*, 206(1):311–333.
- Begnudelli, L. and Sanders, B. F. (2006). Unstructured Grid Finite-Volume Algorithm for Shallow-Water Flow and Scalar Transport with Wetting and Drying. *Journal of Hydraulic Engineering-asce*, 132.
- Beljadid, A., Mohammadian, A., and Kurganov, A. (2016). Well-balanced positivity preserving cell-vertex central-upwind scheme for shallow water flows. *Computers & Fluids*.
- Benkhaldoun, F., Sahmim, S., and Seaid, M. (2010). A two-dimensional finite volume morphodynamic model on unstructured triangular grids. *International Journal for Numerical Methods in Fluids*, 63(11):1296–1327.
- Benkhaldoun, F., Seaid, M., and Sahmim, S. (2011). Mathematical development and verification of a finite volume model for morphodynamic flow applications. *Advances in Applied Mathematics and Mechanics*, 3:470–492.
- Bilanceri, M., Beux, F., Elmahi, I., Guillard, H., and Salvetti, M. V. (2010). Linearised implicit time-advancing applied to sediment transport simulations. Rapport de recherche RR-7492, INRIA.
- Bollermann, A., Chen, G., Kurganov, A., and Noelle, S. (2013a). A well-balanced reconstruction of wet/dry fronts for the shallow water equations. *Journal of Scientific Computing*, 56(2):267–290.
- Bollermann, A., Chen, G., Kurganov, A., and Noelle, S. (2013b). A well-balanced reconstruction of wet/dry fronts for the shallow water equations. *Journal of scientific computing*, 56(2):267–290.
- Bollermann, A., Noelle, S., and Medvidová, M. L. (2015). Finite volume evolution galerkin methods for the shallow water equations with dry beds. *arXiv preprint arXiv:1501.03628*.
- Bradford, S. F. and Sanders, B. F. (2002). Finite-volume model for shallow-water flooding of arbitrary topography. *Journal of Hydraulic Engineering*, 128:289.
- Bryson, S., Epshteyn, Y., Kurganov, A., and Petrova, G. (2011). Well-balanced positivity preserving central-upwind scheme on triangular grids for the saint-venant system. *ESAIM: Mathematical Modelling and Numerical Analysis*, 45(03):423–446.
- Caleffi, V., Valiani, A., and Bernini, A. (2007). High-order balanced {CWENO} scheme for movable bed shallow water equations. *Advances in Water Resources*, 30(4):730 – 741.
- Canestrelli, A., Dumbser, M., Siviglia, A., and Toro, E. F. (2010). Well-balanced high-order centered schemes on unstructured meshes for shallow water equations with fixed and mobile bed. *Advances in Water Resources*, 33(3):291 – 303.
- Canestrelli, A., Siviglia, A., Dumbser, M., and Toro, E. F. (2009). Well-balanced high-order centred schemes for non-conservative hyperbolic systems. applications to shallow water equations with fixed and mobile bed. *Advances in Water Resources*, 32(6):834–844.
- Canestrelli, A. and Toro, E. F. (2012). Restoration of the contact surface in force-type centred schemes i: Homogeneous two-dimensional shallow water equations. *Advances in Water Resources*, 47:88–99.
- Cao, Z. and Carling, P. (2002). Mathematical modelling of alluvial rivers: reality and myth. part 1: General review. *Proceedings of the ICE-Water and Maritime Engineering*, 154(3):207–219.
- Cao, Z. and Carling, P. A. (2005). Further perspectives on the evolution of bed material waves in alluvial rivers. *Earth Surface Processes and Landforms*, 30(1):115–120.
- Cao, Z., Huang, W., Yue, Z., and Pender, G. (2010). Coupled 2d mathematical modeling of dam break flow over erodible bed-ucl test case. In *NSF-PIRE 2010 Workshop Dam-break flow on mobile bed, private communication at <http://www.uclouvain.be/373040.html>*.

- Cao, Z., Pender, G., Wallis, S., and Carling, P. (2004). Computational dam-break hydraulics over erodible sediment bed. *Journal of Hydraulic Engineering*, 130(7):689–703.
- Cao, Z., Yue, Z., and Pender, G. (2011). Flood hydraulics due to cascade landslide dam failure. *Journal of Flood Risk Management*, 4(2):104–114.
- Capart, H. and Young, D. L. (1998). Formation of a jump by the dam-break wave over a granular bed. *Journal of Fluid Mechanics*, 372:165–187.
- Castro, M. J., Ferreiro, A. F., García-Rodríguez, J. A., González-Vida, J. M., Macías, J., Parés, C., and Vázquez-Cendón, M. E. (2005). The numerical treatment of wet/dry fronts in shallow flows: application to one-layer and two-layer systems. *Mathematical and Computer Modelling*, 42(3):419–439.
- Castro Díaz, M. J., Gallardo, J. M., López-García, J. A., and Parés, C. (2008). Well-balanced high order extensions of Godunov’s method for semilinear balance laws. *SIAM J. Numer. Anal.*, 46(2):1012–1039.
- Cordier, S., Le, M. H., and De Luna, T. M. (2011). Bedload transport in shallow water models: Why splitting (may) fail, how hyperbolicity (can) help. *Advances in Water Resources*, 34(8):980–989.
- Črnjarić-Žic, N., Vuković, S., and Sopta, L. (2004). Extension of eno and weno schemes to one-dimensional sediment transport equations. *Computers & fluids*, 33(1):31–56.
- De Vriend, H. n. (1987). 2dh mathematical modelling of morphological evolutions in shallow water. *Coastal Engineering*, 11(1):1–27.
- Di, M. C., Fernández-Nieto, E., Ferreiro, A., Parés, C., et al. (2009). Two-dimensional sediment transport models in shallow water equations. a second order finite volume approach on unstructured meshes. *Computer Methods in Applied Mechanics and Engineering*, 198(33):2520–2538.
- Fagherazzi, S. and Sun, T. (2003). Numerical simulations of transportational cyclic steps. *Computers and Geosciences*, 29(9):1143 – 1154.
- Field, J. (2001). Channel avulsion on alluvial fans in southern arizona. *Geomorphology*, 37(1):93–104.
- Fraccarollo, L. and Capart, H. (2002). Riemann wave description of erosional dam-break flows. *Journal of Fluid Mechanics*, 461:183–228.
- Grass, A. (1981). Sediment transport by waves and currents. Technical Report FL29, SERC London Cent. Mar. Technol.
- Harten, A. (1983). High resolution schemes for hyperbolic conservation laws. *Journal of Computational Physics*, 49(3):357 – 393.
- He, S., Liu, W., Li, X., and Ouyang, C. (2014). An improved coupling model for water flow, sediment transport and bed evolution (casfe v.1). *Geoscientific Model Development Discussions*, 7(2):2429–2454.
- Hudson, J. and Sweby, P. K. (2005). A high-resolution scheme for the equations governing 2d bed-load sediment transport. *International Journal for Numerical Methods in Fluids*, 47(10-11):1085–1091.
- Huynh, H. (2003). Analysis and improvement of upwind and centered schemes on quadrilateral and triangular meshes. *AIAA Paper*, 3541:23–26.
- Jiang, G., Levy, D., Lin, C., Osher, S., and Tadmor, E. (1998). High-resolution nonoscillatory central schemes with nonstaggered grids for hyperbolic conservation laws. *SIAM Journal on Numerical Analysis*, 35(6):2147–2168.
- Jiang, G.-S. and Tadmor, E. (1998). Nonoscillatory central schemes for multidimensional hyperbolic conservation laws. *SIAM J. Sci. Comput.*, 19:1892–1917.
- Kesserwani, G. and Liang, Q. (2010). Well-balanced rkdg2 solutions to the shallow water equations over irregular domains with wetting and drying. *Computers & Fluids*, 39(10):2040–2050.

- Kleinhans, M. G., Ferguson, R. I., Lane, S. N., and Hardy, R. J. (2013). Splitting rivers at their seams: bifurcations and avulsion. *Earth Surface Processes and Landforms*, 38(1):47–61.
- Kurganov, A. and Levy, D. (2002). Central-upwind schemes for the saint-venant system. *ESAIM: Mathematical Modelling and Numerical Analysis*, 36(03):397–425.
- Kurganov, A. and Lin, C.-T. (2007). On the reduction of numerical dissipation in central-upwind schemes. *Commun. Comput. Phys*, 2(1):141–163.
- Kurganov, A., Petrova, G., et al. (2007). A second-order well-balanced positivity preserving central-upwind scheme for the saint-venant system. *Communications in Mathematical Sciences*, 5(1):133–160.
- Kurganov, A. and Tadmor, E. (2000). New high-resolution central schemes for nonlinear conservation laws and convection–diffusion equations. *Journal of Computational Physics*, 160(1):241–282.
- LeVeque, R. J. (1998). Balancing source terms and flux gradients in high-resolution godunov methods: the quasi-steady wave-propagation algorithm. *Journal of computational physics*, 146(1):346–365.
- LeVeque, R. J. (2002). *Finite volume methods for hyperbolic problems*, volume 31. Cambridge university press.
- Li, S. and Duffy, C. J. (2011). Fully coupled approach to modeling shallow water flow, sediment transport, and bed evolution in rivers. *Water Resources Research*, 47(3):n/a–n/a.
- Liu, X., Landry, B., and Garcia, M. (2008). Two-dimensional scour simulations based on coupled model of shallow water equations and sediment transport on unstructured meshes. *Coastal Engineering*, 55(10):800–810.
- Liu, X., Mohammadian, A., Kurganov, A., and Sedano, J. A. I. (2015). Well-balanced central-upwind scheme for a fully coupled shallow water system modeling flows over erodible bed. *Journal of Computational Physics*, 300:202–218.
- Nessyahu, H. and Tadmor, E. (1990). Non-oscillatory central differencing schemes for hyperbolic conservation laws. *J. Comp. Phys*.
- Nicholas, A. (2013a). Morphodynamic diversity of the world’s largest rivers. *Geology*, 41(4):475–478.
- Nicholas, A. P. (2013b). Modelling the continuum of river channel patterns. *Earth Surface Processes and Landforms*, 38(10):1187–1196.
- Paola, C. and Voller, V. (2005). A generalized exner equation for sediment mass balance. *Journal of Geophysical Research: Earth Surface (2003–2012)*, 110(F4).
- Postma, G., Kleinhans, M., Meijer, P., and Eggenhuisen, J. (2008). Sediment transport in analogue flume models compared with real-world sedimentary systems: A new look at scaling evolution of sedimentary systems in a flume. *Sedimentology*, 55(6):1541–1557.
- Pudasaini, S. P. and Hutter, K. (2007). *Avalanche dynamics: dynamics of rapid flows of dense granular avalanches*. Springer.
- Ricchiuto, M. (2011). On the c-property and generalized c-property of residual distribution for the shallow water equations. *Journal of Scientific Computing*, 48(1-3):304–318.
- Rogers, B. D., Borthwick, A. G., and Taylor, P. H. (2003). Mathematical balancing of flux gradient and source terms prior to using roe’s approximate riemann solver. *Journal of Computational Physics*, 192(2):422–451.
- Simpson, G. and Castelltort, S. (2006). Coupled model of surface water flow, sediment transport and morphological evolution. *Comput. Geosci.*, 32(10):1600–1614.

- Siviglia, A., Stecca, G., Vanzo, D., Zolezzi, G., Toro, E. F., and Tubino, M. (2013). Numerical modelling of two-dimensional morphodynamics with applications to river bars and bifurcations. *Advances in Water Resources*, 52:243–260.
- Smith, N. D. (1974). Sedimentology and bar formation in the upper kicking horse river, a braided outwash stream. *The Journal of Geology*, pages 205–223.
- Stecca, G., Siviglia, A., and Toro, E. F. (2012). A finite volume upwind-biased centred scheme for hyperbolic systems of conservation laws. applications to shallow water equations. *Communications in Computational Physics*, 12(4):1183–1214.
- Sweby, P. K. (1984). High resolution schemes using flux limiters for hyperbolic conservation laws. *SIAM Journal on Numerical Analysis*, 21(5):pp. 995–1011.
- Toro, E. F. (2001). *Shock-capturing methods for free-surface shallow flows*. John Wiley, Chichester, New York.
- Črnjarić Žic, N., Vuković, S., and Sopta, L. (2004). Balanced finite volume weno and central weno schemes for the shallow water and the open-channel flow equations. *J. Comput. Phys.*, 200(2):512–548.
- Wang, Y., Hutter, K., and Pudasaini, S. (2004). The savage-hutter theory: A system of partial differential equations for avalanche flows of snow, debris, and mud. *ZAMM - Journal of Applied Mathematics and Mechanics / Zeitschrift für Angewandte Mathematik und Mechanik*, 84(8):507–527.
- Xia, J., Lin, B., Falconer, R. A., and Wang, G. (2010). Modelling dam-break flows over mobile beds using a 2d coupled approach. *Advances in Water Resources*, 33(2):171–183.
- Yang, C. T. (2006). Erosion and sedimentation manual. *US Dep. of the Interior, Bureau of Reclamation, Denver, CO*.
- Yue, Z., Cao, Z., Li, X., and Che, T. (2008a). Two-dimensional coupled mathematical modeling of fluvial processes with intense sediment transport and rapid bed evolution. *Science in China Series G: Physics, Mechanics and Astronomy*, 51(9):1427–1438.
- Yue, Z., Cao, Z., Li, X., and Che, T. (2008b). Two-dimensional coupled mathematical modeling of fluvial processes with intense sediment transport and rapid bed evolution. *Science in China Series G: Physics, Mechanics and Astronomy*, 51(9):1427–1438.
- Zia, H. (2015). *A numerical model for simulating sediment routing in shallow water flow*. PhD thesis, University of Geneva.
- Zia, H. (under-review2016). Well-balanced, anti-diffusive non-oscillatory central difference (adnoc) scheme for the shallow water equations with wet-dry fronts. *Computers & Fluids*.
- Zoppou, C. and Roberts, S. (2003). Explicit schemes for dam-break simulations. *Journal of Hydraulic Engineering*, 129:11.

List of Figures

1	Staggered grid with grid points marked by \circ and \bullet for the two different grids. The cell centers of the contributing sub-cells are marked by \blacksquare	26
2	1D dam break on erodible bed. Water depth and bed morphology, 60 sec. after dam break.	27
3	Two dimensional dam break experiment.	28
4	Evolution of a conical dune. Bed topography after 100 hours.	29
5	Stratigraphic development in the 1D flume experiment.	30
6	Dynamic bed forms in a two dimensional numerical flume calculated with the adNOC scheme.	31

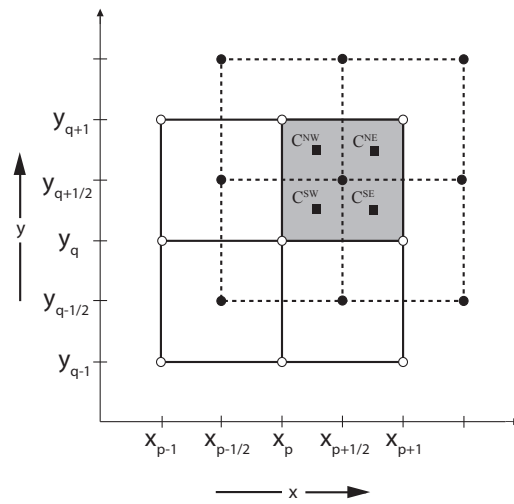


Figure 1: Staggered grid with grid points marked by \circ and \bullet for the two different grids. The cell centers of the contributing sub-cells are marked by \blacksquare .

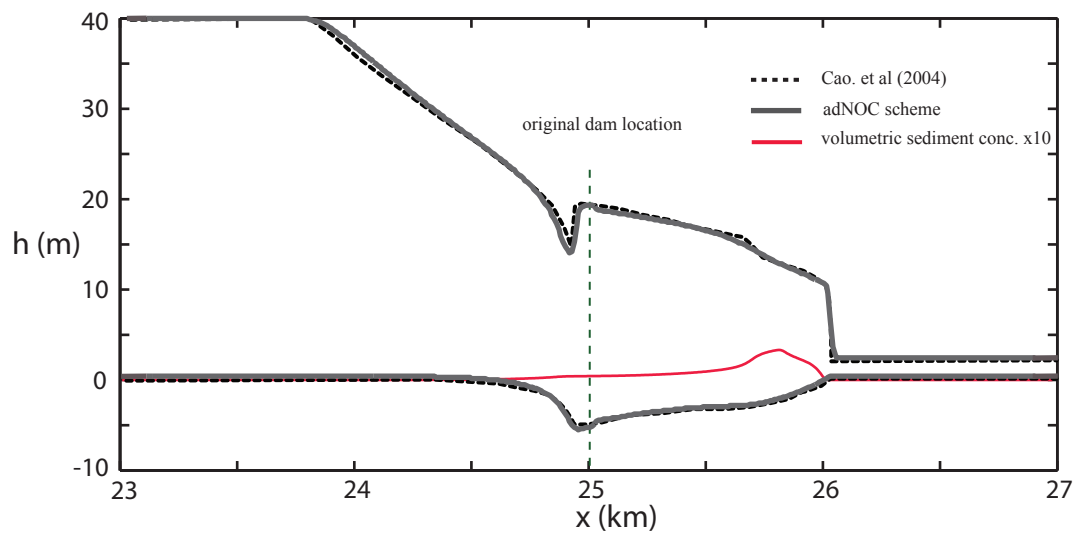
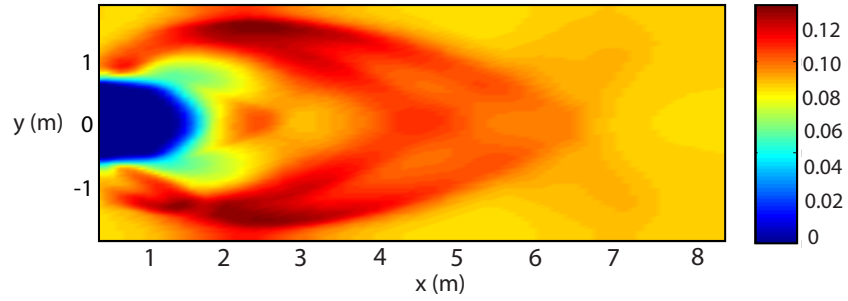
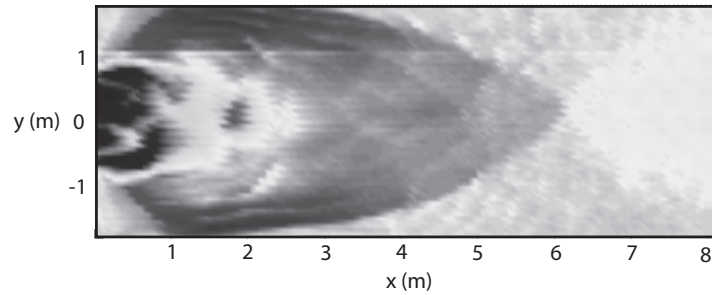


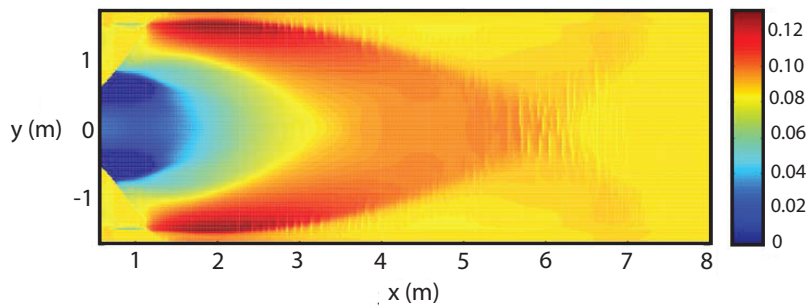
Figure 2: 1D dam break on erodible bed. Water depth and bed morphology, 60 sec. after dam break.



(a) Bed topography 20 sec. after the dam breach calculated using the *adNOC* scheme.



(b) Bed topography 20 sec. after the dam breach determined from a flume experiment (published by (Cao et al., 2010)).



(c) Bed topography 20 sec. after the dam breach as calculated using a Riemann-solver based method (published by (Cao et al., 2010)).

Figure 3: Two dimensional dam break experiment.

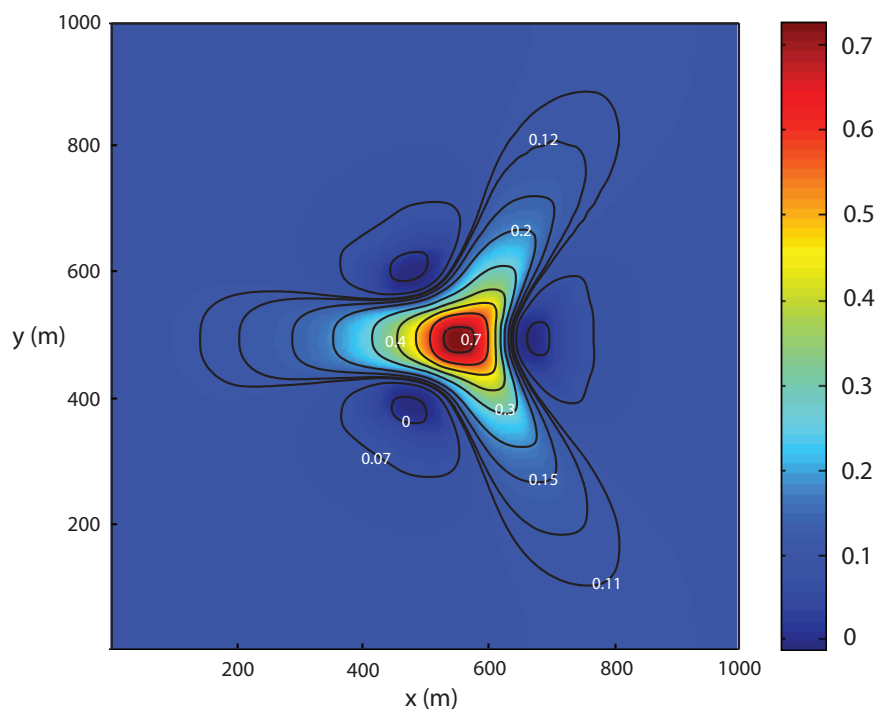
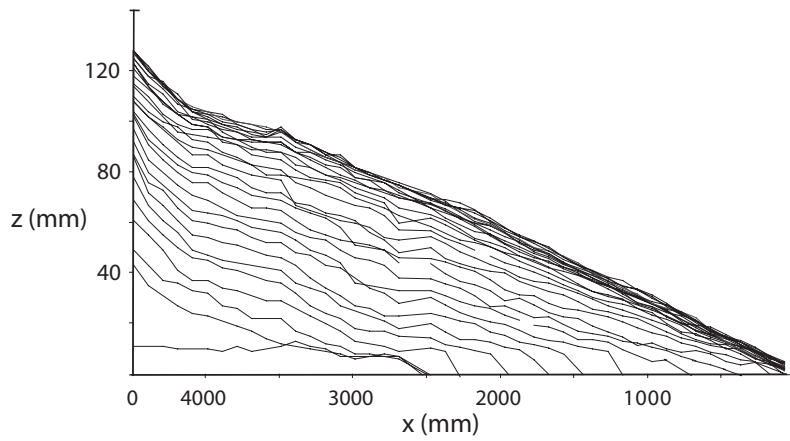
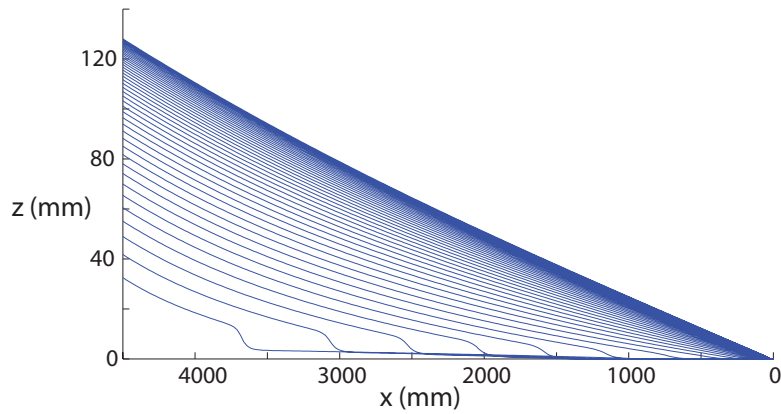


Figure 4: Evolution of a conical dune. Bed topography after 100 hours.



(a) Stratigraphic development of the fluvial sediment wedge in a flume (published by (Postma et al., 2008)). Each line is drawn after one hour.



(b) Stratigraphic development as calculated by the morphodynamic model using the adNOC scheme. Each line is drawn after one hour.

Figure 5: Stratigraphic development in the 1D flume experiment.

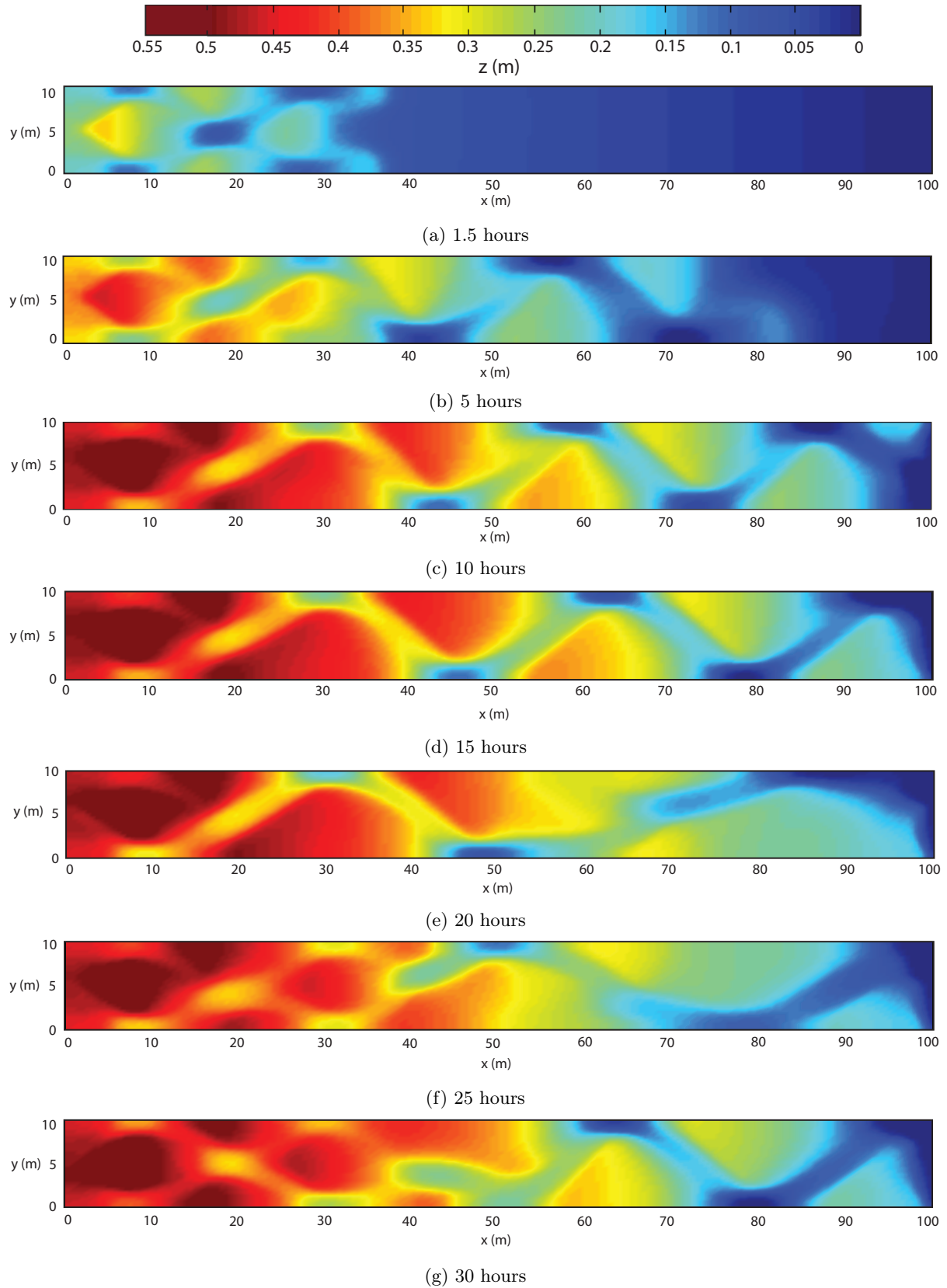


Figure 6: Dynamic bed forms in a two dimensional numerical flume calculated with the adNOC scheme.

List of Tables

1	List of notation used, with units in brackets where applicable.	20
2	Parameter values used in the test cases. Units are shown in brackets where applicable.	33

Parameter	dam break 1d	dam break 2d	conical dune	sediment wedge	flume experiment
g (m/s^2)	9.8	9.8	9.8	9.8	9.8
i	2.0	2.0	-	-	2.0
ν (m^2/s)	1.2×10^{-6}	1.2×10^{-6}	-	-	1.2×10^{-6}
ϕ	0.4	0.42	0.4	0.4	0.4
n	0.03	0.0165	0	0.082	0.033
s	1.63	1.63	-	-	1.63
θ_c	0.045	0.045	-	-	0.045
d (mm)	8	1.61	-	-	1
f	0.03	0.03	-	-	0.03
ε (shallow water system)	0.6	0.6	0.3	0	0
ε (suspended transport)	0.6	0.5	-	-	0
ε (Exner's equation)	1	0.9	1	0.995	0.92
ζ	1	0.01	0	0	0.5
A	0	0.0001	0.001	0.04	0.001
b	-	3	3	4	3
Δx (m)	10	0.09	5	0.0225	0.5
Δy (m)	-	0.036	5	-	0.33
Cn	0.5	0.4	0.5	0.5	0.45

Table 2: Parameter values used in the test cases. Units are shown in brackets where applicable.